第 36 卷第 6 期
2020 年 6 月

无 机 化 学 学 报
CHINESE JOURNAL OF INORGANIC CHEMISTRY

Vol.36 No.6
1113-1122

用于活体和细胞内 SO_2 衍生物检测的线粒体靶向双光子磷光铱(Ⅲ)配合物

赵子建# 侯明萱# 王康男* 刘柳宜 毛宗万*
(中山大学化学学院,生物无机与合成化学教育部重点实验室,广州 510275)

摘要:暴露于高剂量的二氧化硫(SO_2)及其衍生物(SO_3^{2-}和 HSO_3^-)会导致血管疾病甚至肺癌发生。双光子磷光成像显微术(TPPIM)和双光子磷光寿命成像显微术(TPPLIM)具有良好的时空分辨能力、抗光漂白、抗自体荧光以及较强组织穿透性等优点,可以实现 SO_2 衍生物在生物样品中实时检测。得益于铱配合物的长磷光寿命(~110 ns)和线粒体靶向特性,本文报道了首例基于 TPPLIM 技术的 SO_2 衍生物检测探针 **Ir-EA**。**Ir-EA** 对水溶液中的亚硫酸氢盐表现出高特异性和灵敏性的识别能力(69 倍磷光增强,10 倍亚硫酸氢盐)和较低的检测限(65 nmol·L^{-1})。更为重要的是,**Ir-EA** 对活细胞和斑马鱼的线粒体中 SO_2 衍生物表现出良好的成像效果。

关键词:二氧化硫衍生物;双光子磷光寿命成像;铱配合物;线粒体靶向;斑马鱼
中图分类号:O614.82+5 **文献标识码**:A **文章编号**:1001-4861(2020)06-1113-10
DOI:10.11862/CJIC.2020.124

Mitochondria-Targeted Iridium(Ⅲ) Complex Used as a Two-Photon Phosphorescent Probe for SO_2 Derivatives Detection *in Vitro* and *in Vivo*

ZHAO Zi-Jian# HOU Ming-Xuan# WANG Kang-Nan* LIU Liu-Yi MAO Zong-Wan*
(*MOE Key Laboratory of Bioinorganic and Synthetic Chemistry, School of Chemistry, Sun Yat-sen University, Guangzhou* 510275, *China*)

Abstract: Exposure to high doses of sulfur dioxide (SO_2) derivatives (SO_3^{2-} and HSO_3^-) are associated with many cardiovascular diseases and lung cancer. Benefiting from the advantages of two-photon phosphorescence imaging microscopy (TPPIM) even two-photon phosphorescence lifetime imaging microscopy (TPPLIM), including excellent spatial and temporal resolutions, anti-photobleaching, anti-autofluorescence, and strong penetration, could be promising features for real-time detection of biological bisulfite derivatives in living tissues. Herein, we firstly report the probe (named as **Ir-EA**) for SO_2 derivatives based on TPPLIM technology. **Ir-EA** was developed with an iridium complex according to its long phosphorescence lifetime (~110 ns) and the mitochondrial targeting properties. More importantly, **Ir-EA** displayed a significant luminescence enhancement (69-fold, 10 eq.) and a low detection limit (65 nmol·L^{-1}) for bisulfite in an aqueous solution. Additionally, **Ir-EA** can selectively lighting-up mitochondria bisulfite derivatives in living cells as well as zebrafish. CCDC: 1914016, **Ir-EA**.

Keywords: biological bisulfite; two-photon phosphorescence lifetime imaging microscopy; iridium(Ⅲ) complex; mitochondria-targeted; zebrafish

收稿日期:2020-02-05。收修改稿日期:2020-03-23。
国家自然科学基金(No.21837006),教育部创新团队(IRT-17R111),中央高校基本科研业务费专项资金,中国博士后科学基金(No.2019M662968),广东省基础与应用基础研究基金联合基金(No.2019A1515110356)和广东省大学生科技创新培育专项资金(No.pdjha0005)资助项目。
#共同第一作者。
*通信联系人。E-mail:wangkn3@mail2.sysu.edu.cn,cesmzw@mail.sysu.eddu.cn

0 Introduction

Sulfur dioxide (SO_2) is among the air pollutants, which combines with water, forming sulfuric acid- the main component of acid rain[1-3]. Once SO_2 inhaled into the human body, it produces sulfite and bisulfite[4], which can further lead to lower respiratory infection (*e.g.* bronchitis, pneumonia), even lung cancer[5]. In neutral fluid and plasma, SO_2 is broken down to its derivatives, sulfite and bisulfite (3:1)[6] with a total sulfite concentration of 0~9.85 $\mu mol \cdot L^{-1}$ measured in serum samples[7]. However, serum sulfite levels are markedly increased in patients with acute pneumonia and renal failure[8]. Endogenous bisulfite derivatives are generated from the metabolism of *L*-cysteine; and aspartate aminotransferase (AAT) (the key enzyme for production of bisulfite derivatives[9]), is overexpressed in cytosol and mitochondria[10]. Exposure to high doses of SO_2 levels are linked with many cardiovascular diseases and lung cancer[11]. SO_2 and bisulfite derivatives play an important role in mammalian organisms[12] and are considered among the so called gasotransmitters, such as NO, CO and H_2S[13-14]. Therefore, it is important and significant to illustrate the formation and biological roles of SO_2 and its derivatives by a powerful molecular sensor. However, there are still many challenges in real-time detection of bisulfite derivatives in biological samples[7,15-16].

Generally, SO_2 and its bisulfite derivatives have been determined using high-performance liquid chromatography, ultraviolet-visible absorption spectrophotometry, mass spectrometry, capillary electrophoresis, and potentiometry[17-21]. Compared with the aforementioned techniques, fluorescence imaging has a number of advantages, such as robust response, high sensitivity, real-time and visual detection in living cells and biological tissues[22-23]. However, current fluorescent imaging probes suffer from shallow tissue penetration, high photodamage, and autofluorescence background interference, which limit their *in vivo* applications for rapid detection of biological targets. In contrast, both two-photon imaging microscopy (TPIM) and two-photon lifetime imaging microscopy (TPLIM), have excellent spatial and temporal resolution, anti-photobleaching, non-invasive, low phototoxicity, strong penetration, and higher resolution[24-29]. Despite these advantages, their applications are still limited. It has to be noted that the lifetime of traditional two-photon organic small molecule fluorescent dye at nanosecond timescale, is similar to cellular background autofluorescence (usually less than 10 ns), which in turn could limit their contrast and sensitivity. These challenges have urged us to develop more effective imaging materials.

Phosphorescent metal-based materials have the advantages of high luminescence quantum yield, long-lived phosphorescence, and large stokes shift [30-31]. Phosphorescent iridium complexes, as a typical phosphorescent reagent, are representative luminescent probes for phosphorescence lifetime imaging microscopy (PLIM) with lifetimes at microsecond timescale. PLIM has attracted great attention in biosensing and bioimaging, owing to its excellent photophysical properties[32-33]. Two-photon phosphorescence lifetime imaging microscopy (TPPLIM) that uses the near-infrared (NIR) light as excitation source, which has deep penetration depth can effectively eliminate the background influence and demonstrates micro-environmental variations of the chromophore in a quantitative manner[34-35]. As reported, the iridium complexes are sensitive to diverse cellular microenvironment variations, such as pH[32], oxygen[36], viscosity[37], and metal ions[38]. Although the iridium complexes as phosphorescent probes have been developed for detecting bisulfites derivatives[39-44], it is worth noting that no TPPLIM probe for visualization of the generated SO_2 derivatives in mitochondria has been reported.

Herein, we present a long life-time (~110 ns) reactive phosphorescent cyclometalated iridium (Ⅲ) complex probe (named as **Ir-EA**) for detecting sulfur dioxide (SO_2) derivatives (SO_3^{2-} and HSO_3^-) *in vitro* and *in vivo* (Scheme 1). The reactivity of bisulfite toward **Ir-EA** probe (through Michael addition reaction) was sensitive over the other biologically relevant active small molecules in the light of significant luminescence enhancement, incre-ases in

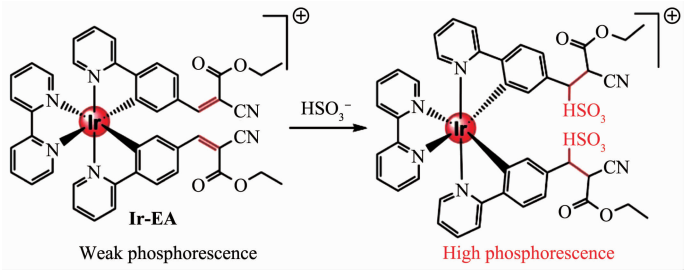

Scheme 1　Schematic reaction mechanism between bisulfite and **Ir-EA**

the lifetime of phosphorescent, and extremely low detection limit in aqueous solution [45-47]. Interestingly, **Ir-EA** is preferentially accumulated in the mitochondria due to its lipophilic-cationic characteristics and thence can detect bisulfites derivatives in real time at subcellular level with superior two-photon effect. More importantly and compared to previous reports, **Ir-EA** has been greatly improved in terms of cytotoxicity [40], selectivity [41], and sensitivity [42] (Table S1), which are more appropriate for real-time detection of biological bisulfite derivatives at long-time term. Our work provides a novel example for the design and potential application of TPPLIM probe for the detection of bisulfite in the circumstance of *in vitro* and *in vivo* phosphorescence imaging.

1　Experimental

1.1　Synthesis and characterization

All solvents (analytical grade) and reagents were purchased from commercial sources unless otherwise specified. The compounds $[Ir(ppy\text{-}CHO)_2Cl]_2$ and **L-EA** were synthesized according to literature procedure[48-49].

Synthesis of $[Ir(ppy\text{-}CHO)_2(bpy)]PF_6$: $[Ir(ppy\text{-}CHO)_2Cl]_2$ (1.70 g, 1.43 mmol) and 2,2′-bipyridine (466 mg, 3.00 mmol) were mixed with 30 mL CH_2Cl_2 and then allowed to cool at r.t. after stirring for 6 h at 65 ℃ under nitrogen. Afterward, NH_4PF_6 (2.40 g, 14.72 mmol) was added and stirred a further 4 h for anion exchange. Next, the filtrate was evaporated, and 10 mL anhydrous ether was added for typical precipitation. After filtration, drying, and purification (using silica gel column chromatography), 1.99 g of yellow solid was obtained. Yield: 81.03%.

Synthesis of **Ir-EA**: $[Ir(ppy\text{-}CHO)_2(bpy)]PF_6$ (0.50 g 0.58 mmol) and ethyl cyanoacetate (68 mg, 0.60 mmol) were dissolved in 35 mL ethanol, 20 μL piperidine was added, and the mixture was stirred at 40 ℃ for 5 h. The filtrate was obtained under reduced pressure, and 377 mg orange red solid was collected after purification through silica gel column chromatography with CH_2Cl_2 and CH_3OH as eluant (50∶1 to 10∶1, *V*/*V*). Yield: 61.72%.

^1H NMR (400 MHz, DMSO-d_6): δ 8.78 (d, *J*=8.2 Hz, 2H), 8.34 (d, *J*=8.2 Hz, 2H), 8.29~8.21 (t, 2H), 8.14~8.06 (t, 6H), 8.03~7.96 (t, 2H), 7.92 (d, *J*=5.4 Hz, 2H), 7.66 (t, *J*=6.4 Hz, 4H), 7.56 (d, *J*=8.3, 1.5 Hz, 2H), 7.23 (t, *J*=12.8, 6.6 Hz, 2H), 7.09 (s, 2H), 4.25 (q, *J*=7.1 Hz, 4H), 1.25 (t, *J*=7.1 Hz, 3H). ^{13}C NMR (101 MHz, DMSO-d_6): δ 165.37 (s), 162.40 (s), 156.01 (s), 154.98 (s), 150.48 (s), 150.06 (s), 149.85 (s), 149.70 (s), 140.59 (s), 139.72 (s), 132.74 (s), 132.54 (s), 129.42 (s), 127.56 (s), 126.26 (s), 125.70 (s), 122.51 (s), 115.79 (s), 102.65 (s), 62.71 (s), 14.42 (s). ESI-MS (MeOH): *m*/*z* Calcd. for $[M-PF_6]^+$, 903.01; Found: 903.46.

1.2　Crystallographic structure determination

Diffusion of diethyl ether into the CH_3OH solution got the crystals of **Ir-EA** qualified for X-ray analysis at room temperature. X-ray diffraction measurements were carried out on a Bruker Smart 1000 CCD diffractometer with Cu *Kα* radiation (λ= 0.154 178 nm) at 150 K. The crystal structures of **Ir-EA** were solved through direct methods with program SHELXS and refined by the full-matrix least-squares program SHELXL[50].

CCDC: 1914016.

1.3　Procedures for spectra measurement

Stock solution of **Ir-EA** (20 mmol·L^{-1}) was dissolved in DMSO and diluted to final concentration (20 μmol·L^{-1}) with test solvent prior to application. After 5 min stabilization in quartz cells (1 cm×1 cm),

all electronic absorption and emission spectra were recorded. Stock solution of bisulfite was obtained at a concentration of 50 mmol·L^{-1}.

1.4 Confocal imaging

For live cell confocal laser scanning microscopy experiment, cells were first seeded in a glass dish at a density of 1×10^4 cells and then incubated for 48 h, cell images were captured with Carl Zeiss LSM 710 confocal microscopy.

1.5 *In vivo* imaging of zebrafish larvae

Zebrafish larvae were bred in zebrafish embryo culture media for two days after hatching. The healthy larvae were selected and incubated with **Ir-EA** (5 μmol·L^{-1}) for 2 h and/or additional treatment with bisulfite (50 μmol·L^{-1}) before visualized using confocal microscopy (λ_{ex}=810 nm (TPPIM); λ_{em}=(600±20) nm).

2 Results and discussion

2.1 Chemical synthesis and characterization

Ir-EA was synthesized according to literature methods (Scheme S1)[48-49] and characterized by ^{1}H nuclear magnetic resonance (NMR), ^{13}C NMR, electrospray ionization mass spectrometry (ESI-MS) (Fig.S1~S5), and X-ray crystallography (Scheme 1 and Table S2). The absorption and phosphorescence spectra of **Ir-EA** in phosphate buffer saline (PBS), CH_3CN, and CH_2Cl_2 are characterized as shown in Fig. S6 and Table S3. The mechanism of phosphorescence quenching in **Ir-EA** is mostly attributed to the strong electron-withdrawing groups[51-52]. Upon excitation at 405 nm, **Ir-EA** was stimulated to produce weak red phosphorescence at 700 nm in PBS (Fig.S6B) with low phosphorescence quantum yields (0.22%) and short phosphorescent lifetimes (Table S3). The solubility of **Ir-EA** in a given solvent is largely a function of the polarity of the solvent, which is considered as a source of variation in properties.

2.2 Detection of sulfur dioxide derivatives in aqueous solution

As shown in Fig.1A, we first examined the spectral signal response of **Ir-EA** toward bisulfite. **Ir-EA** exhibited intense absorption in the region between 230 and 280 nm with the highest absorption band at 250 nm (ε=3.43×10^4 L·mol^{-1}·cm^{-1}) and 350 nm (ε=

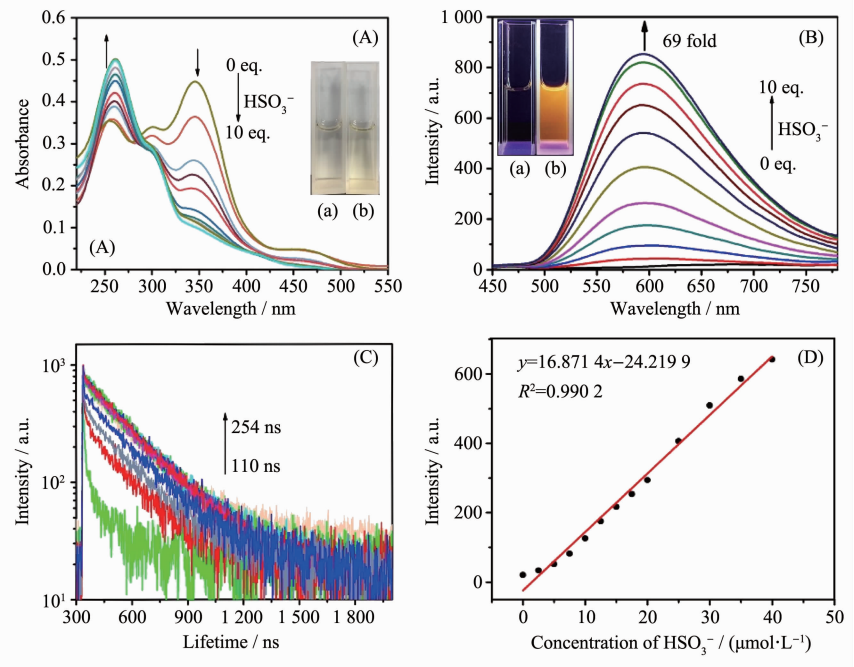

Inset: **Ir-EA** solution in the absence or presence of HSO_3^- observed by natural light (A) or under 365 nm UV lamp (B)

Fig.1 Changes in UV-Vis absorption (A) and emission (B) spectra of **Ir-EA** with the addition of increasing HSO_3^- in PBS/DMSO (9:1, *V*/*V*) solution (λ_{ex}=405 nm); (C) Changes in the luminescence lifetime of **Ir-EA** with the addition of increasing HSO_3^-; (D) Phosphorescence intensity changes at 600 nm of **Ir-EA** depend on the concentration of HSO_3^-

4.43×10^4 $L\cdot mol^{-1}\cdot cm^{-1}$), in a mixed solution of PBS/DMSO (9:1, *V*/*V*). With the addition of bisulfite into the solution of **Ir-EA**, the original absorption peak at 350 nm gradually decreased with simultaneous increase in the absorption band centered at 250 nm, with isosbestic point observed at 285 nm. The reaction was gradually saturated when 10 equivalent bisulfites were added. Under visible light irradiation, the color of solution gradually changed from yellow to clear colorless (Inset of Fig.1A). As shown in Fig.1B, upon the addition of increasing bisulfite, the intensity of phosphorescence located at 600 nm was enhanced significantly, displaying a *ca.* 69-fold enhancement at $c_{HSO_3^-}$=100 $\mu mol\cdot L^{-1}$. The change could be seen with the naked eye. Phosphorescence of the **Ir-EA** solution gradually changed to bright yellow (from colorless) upon irradiation with 365 nm UV light. More importantly, upon addition of bisulfite in a range of 0~40 $\mu mol\cdot L^{-1}$ (R^2 =0.990), the phosphorescence intensity of **Ir-EA** increased linearly (Fig.1D) and then gradually reached a plateau with increasing bisulfite concentration (Fig.S7). It is worth mentioning that the detection limit of **Ir-EA** was calculated to be 65 $nmol\cdot L^{-1}$ for bisulfite at a signal-to-noise ratio (S/N) of 3. The value is lower than most of iridium probes used to detect bisulfite derivatives (Table S1). Fig.S8 shows that the reaction can be completed within 5 min at 50 $\mu mol\cdot L^{-1}$ bisulfite concentration and the kinetic constants k =0.018 4 s^{-1}, which indicates that **Ir-EA** has a short response time to bisulfite. We also explored the changes in the phosphorescence lifetimes (PL) of **Ir-EA** at a range of 0~10 eq. (0~100 $\mu mol\cdot L^{-1}$) of bisulfite. With the addition of bisulfite, the PL of **Ir-EA** increased from 110 to 254 ns (Fig.1C), which is much longer than typical organic probes (usually less than 10 ns). The significant change of lifetime makes it possible to strongly avoid auto-fluorescent background through TPPLIM[37].

2.3 Specificity of Ir-EA for bisulfite derivatives

We next examined the specificity of **Ir-EA** for bisulfite derivatives. In addition to bisulfite derivatives, there are several sulfur-containing substances, such as bio-thiol, hydrogen sulfide, and thiocyanate ion in cells, which may have great influence on the specific recognition of **Ir-EA** toward bisulfite derivatives[53-54]. In order to eliminate the possible influence of these interferences, we investigated the specificity of **Ir-EA** for detecting bisulfite derivatives in solution environment. In the presence of various reactive sulfur species (S^{2-}, HS^-, and SCN^-), reactive oxygen species (H_2O_2 and ClO^-), bio-relevant species (GSH and Cys), common anions (CO_3^{2-}, CH_3COO^-, $C_2O_4^{2-}$,$H_2PO_4^-$, HPO_4^{2-}, NO_3^-, NO_2^-, NH_4^+, OH^-, F^-, Cl^-, ClO_4^-, SO_4^{2-}, $S_2O_3^{2-}$, CN^-, EDTA, and citric acid), and several metal cations (Ca^{2+}, Al^{3+}, Zn^{2+}, Fe^{3+},Fe^{2+}, Cu^{2+}, Mn^{2+},and Co^{3+}) at a high concentration (1 $mmol\cdot L^{-1}$), the phosphorescence intensity was recorded after it was stable. As shown in Fig.S9, all these disturbing reactive species could not induce an obvious change in the emission of **Ir-EA** and similar rapid enhancement of phosphorescence intensity was observed after addition of bisulfite. To further specify the specificity of **Ir-EA** towards bisulfite, we also evaluated the phosphorescent response to pH. In the absence of bisulfite, the phosphorescence intensity of **Ir-EA** was weak and stable at pH value range of 4.5~8.5 (Fig.S10). Upon addition of bisulfite, there was still a significant enhancement of the phosphorescence intensity after reacting with bisulfite. Therefore, at the physiological pH[55], there was a minimal affection of phosphorescent response of **Ir-EA**. All these results suggest that **Ir-EA** is a specific, highly sensitive bioprobe and has the potential to detect bisulfite in biological environments.

2.4 Sensing mechanism of Ir-EA for bisulfite derivatives

To investigate the sensing mechanism, Job′s plot was drawn, and the result indicated the interaction between **Ir-EA** and bisulfite through a 1:2 binding ration (Fig.S11). Additionally, the ESI-MS of **Ir-EA** after reaction with bisulfite showed new peaks at 1 111.21 (Fig.S12), suggesting that the addition products reacted with two bisulfite (*m*/*z*=1 111.12 *ca.* for [**Ir-EA** $-PF_6+2NaSO_3]^+$). To investigate the reaction process[56] and verify the additive position (Scheme 1B), the structural change of ligand **L-EA** reacted with bisulfite

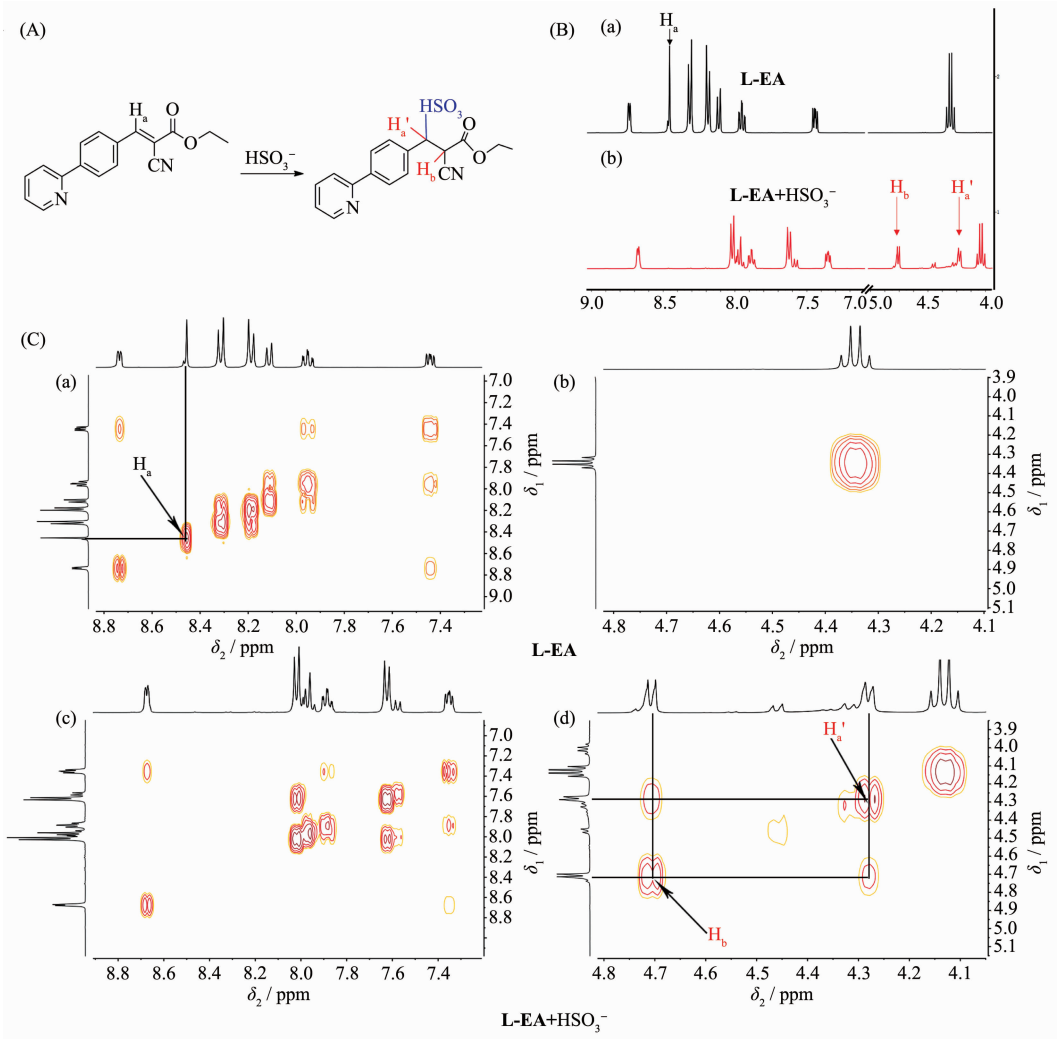

Fig.2 Schematic reaction of bisulfite with **L-EA** (A); Partial ^{1}H NMR (B) and 2D COSY (C) spectrum of **L-EA** upon addition of bisulfite (5 eq.) in DMSO-d_6/D_2O (4:1, *V*/*V*)

was monitored by ^{1}H NMR spectrum and 2D COSY spectrum. The proton signal of double bond in **L-EA** (H_a at δ 8.45) was vanished with the addition of bisulfite to **L-EA** in DMSO-d_6/D_2O (4:1, *V*/*V*) (Fig.2B). In the meantime, two new double peaks (H_a' at δ 4.28, H_b at δ 4.70) appeared, which correspond to change in the chemical shift of protons in original double bond and the new protons obtained by the addition reaction. The results in the 2D COSY spectrum also confirm that the two protons are adjacent, and thereby inferring that the bisulfite was added to carbon atoms attached to benzene in double bond (Fig.2C).

2.5 Intracellular bisulfite imaging

As the basis of bioimaging application, we firstly investigated the cytotoxicity of **Ir-EA** in living cells using 3-(4,5-dimethylthiazol-2-yl)-2,5-diphenyltetrazolium bromide (MTT) assays. MTT data demonstrated that the **Ir-EA** had low cytotoxicity on A549 and HepG2 cells (IC_{50} >100 μmol·L^{-1}; Fig.S13). Mitochondrial membrane potential (MMP) damage is often a momentous marker of apoptosis and other modes of cell death. JC-1 is a commercial probe, which is able to label the MMP specifically. Mitochondrial depolarization leads to a decrease of JC-1 aggregates formation and an increase of monomer, which is indicated by a reduction of the red fluorescence intensity and increases in the green fluorescence intensity. In further MMP experiments, we used a commercial drug carbonyl cyanide *m*-chlorophenyl hydrazine (CCCP), which can lead to mitochondrial

apoptosis, as a positive control. **Ir-EA** did not exhibit a decrease in MMP production 6 h post-incubation in CCCP treated and blank control cells (Fig.S14). These results are consistent with the toxicity data, suggesting that **Ir-EA** has a good biocompatibility.

Subsequently, the distribution of **Ir-EA** in subcellular organelles was checked by colocalization experiments with Mito-Tracker Red (MTR) and Lyso-Tracker Red (LTR) in A549 cells. An excellent overlap between the phosphorescence of **Ir-EA** and that of MTR was viewed (Fig.3A). Additionally, the intensity scatter plots of the two channels (red and green) are overlapped with the Pearson′s colocalization coefficient of 0.86 for **Ir-EA**. Compared with mitochondria, **Ir-EA** is rarely found in lysosomes as imaged by confocal microscopy. These results suggest that **Ir-EA** is mainly located in the mitochondria and thus possess the potential application to detect biological bisulfite derivatives in mitochondria specifically. The significant change of phosphorescent property of **Ir-EA** promoted us to evaluate its further application for bioimaging bisulfite derivatives in living A549 cells. As shown in Fig.S15a, only weak phosphorescence from **Ir-EA** was observed in control. However, a turn-on response of **Ir-EA** toward bisulfite was observed in A549 cells with remarkable phosphorescence enhancement (Fig.S15b~d). Furthermore, the phosphorescent signal can still overlap with MTR (Pearson′s colocalization coefficient: 0.91) (Fig.3B).

Owing to the high sensitivity and selectivity to **Ir-EA** for exogenous detection of bisulfite, its feasibility was then explored to determine endogenous bisulfite in living cells. Thiosulphate sulfurtransferase (TST) is a mitochondrial enzyme involved in the most immediate pathways to generate endogenous bisulfite derivatives from thiosulfate. First, TST react with $Na_2S_2O_3$ to generate a sulfur-substituted enzyme [57-58]. Next, the enzyme-bound sulfur is converted to a thiophilic acceptor, such as glutathione (GSH), to generate thiocyanate or disulfide with the concomitant formation of sulfite or bisulfite. However, TST could be restrained by 2,4,6-trinitrobenzenesulfonate (TNBS)[59-60]. HepG2 cells were treated with $Na_2S_2O_3$/GSH for 2 h to generate the endogenous bisulfite derivatives and then were incubated with **Ir-EA** for an additional 1 h. As depicted in Fig.S16, HepG2 cells treated with either GSH or $Na_2S_2O_3$ in the presence of **Ir-EA** yield a similar phosphorescent intensity compared to the

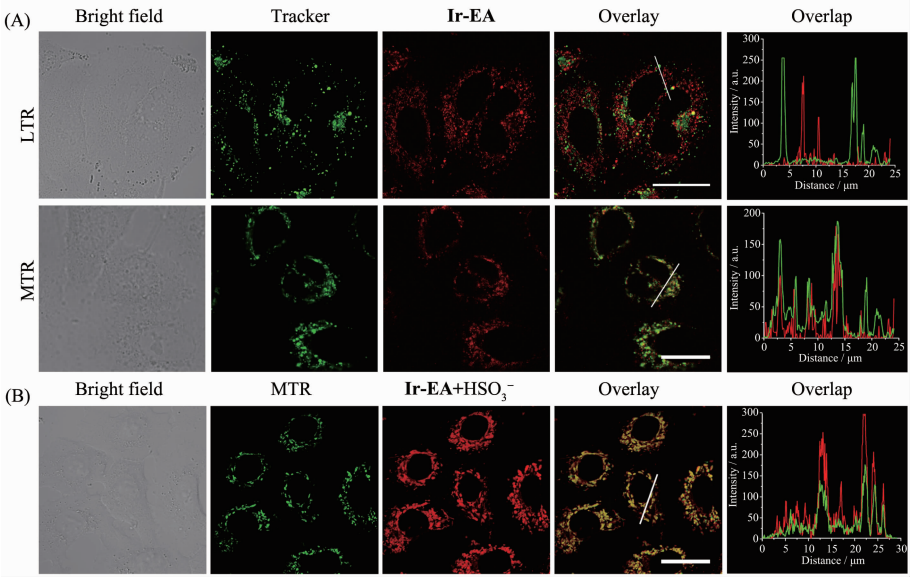

Ir-EA: λ_{ex}=810 nm, λ_{em}=(600±20) nm (red); MTR/LTR: λ_{ex}=543 nm, λ_{em} =(560±10) nm (green); Overlay: overlay of the 2nd and 3rd columns; Scale bars: 20 μm

Fig.3　Colocalization images of A549 cells cultured with **Ir-EA** (10 μmol·L^{-1}, 1 h) and MTR/LTR (100 nmol·L^{-1}, 30 min) (A), and **Ir-EA**+HSO_3^- and MTR (B)

control, which is not a detectable signal. At variance, the phosphorescence intensity was significantly enhanced in HepG2 cells treated with $Na_2S_2O_3$ /GSH by TPPIM (Fig.4A). Additionally, when pre-incubated with TNBS, even HepG2 cells incubated with $Na_2S_2O_3$/GSH could not engender a significant phosphorescent signal (Fig.4A), resulting from that TST was deactivated by TNBS. These imaging results suggest that **Ir-EA** is capable of detecting biological bisulfite derivatives endogenously generated by enzyme in living cells.

TPPLIM effectively eliminates background fluorescence using deep penetrating near infrared (NIR) light excitation, reflecting the micro-environment changes of chromophores[37,61]. The phosphorescence lifetimes of **Ir-EA** toward bisulfite have a significant increase over a timescale of several hundred nanoseconds, which is more versatile than traditional organic fluorescent probes, and are more suitable for TPPLIM. Inspired by this, TPPLIM was also used to investigate the distribution of **Ir-EA** toward bisulfite derivatives in A549 cells. As shown in Fig.4B, the mitochondria of A549 cells (control) exhibit only weak phosphorescence and relatively short lifetimes (109 ns) from **Ir-EA**. However, the mean phosphorescent lifetime (201 ns) was increased when the cells were pre-incubated by GSH (500 μmol·L^{-1}) and $Na_2S_2O_3$ (250 μmol·L^{-1}). The results are in line with those recorded in aqueous (Fig.1C). The application of this method would provide a new strategy to design TPPIM and TPPLIM probes for detection of exogenous and endogenous bisulfites. Subsequent efforts have been expanded to further elucidate the imaging of **Ir-EA** as a phosphorescent probe for sensitive imaging of bisulfite derivatives *in vivo*.

Zebrafish has emerged as an excellent model for genetics and genomics[62-64]. Encouraged by the outstanding imaging effect of **Ir-EA** for endogenous and exogenous bisulfite derivatives in living cells, we further elucidated the application of **Ir-EA** as a sensitive phosphorescent probe for the detection of bisulfite derivatives *in vivo*. As has been observed in Fig.5, there is extremely weak phosphorescence in 2-day-old zebrafish embryo pre-incubated with **Ir-EA** (5 μmol·L^{-1}) for 2 h under confocal microscopy. However, after adding bisulfite (50 μmol·L^{-1}), the phosphorescence was enhanced in zebrafish embryo as shown in the TPPIM images. Therefore, the results of *in vivo* imaging show that **Ir-EA** is capable to enter zebrafish and respond effectively to bisulfite derivatives with no observable toxic effect.

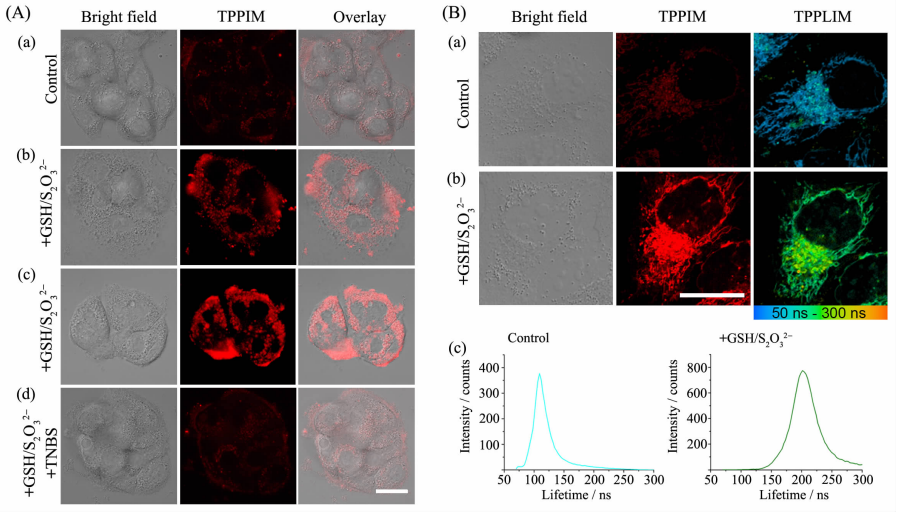

λ_{ex}=810 nm, λ_{em}=(600±20) nm; Scale bars: 20 μm

Fig.4 (A) HepG2 cells stained with 10 μmol·L^{-1} **Ir-EA** (2 h) (a, control), 500 μmol·L^{-1} GSH+250 μmol·L^{-1} $Na_2S_2O_3$ (2 h)+**Ir-EA** (2 h) (b), 1 500 μmol·L^{-1} GSH+750 μmol·L^{-1} $Na_2S_2O_3$ (2 h)+**Ir-EA** (2 h) (c), and 100 mmol·L^{-1} TNBS+1 500 μmol·L^{-1} GSH+750 μmol·L^{-1} $Na_2S_2O_3$ (2 h)+**Ir-EA** (2 h) (d); (B) TPPIM and TPPLIM images of A549 cells stained with 10 μmol·L^{-1} **Ir-EA** (2 h) (a) and 500 μmol·L^{-1} GSH+250 μmol·L^{-1} $Na_2S_2O_3$ (2 h)+**Ir-EA** (2 h) (b)

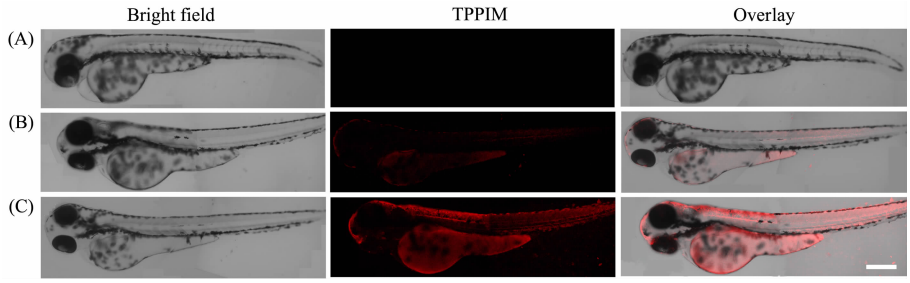

λ_{ex}=810 nm, λ_{em}=(600±20) nm; Scale bars: 200 μm

Fig.5　Two-day-old control zebrafish embryo (A) or pre-incubated with **Ir-EA** (5 μmol·L^{-1}) for 2 h (B), and **Ir-EA** (5 μmol·L^{-1}) for 2 h and then incubated with HSO_3^- (50 μmol·L^{-1}) for 30 min (C)

As we discussed in the introduction, although some iridium complexes have been used for the detection of SO_2 in cells or organisms (Table S1), **Ir-EA** is the first example to take advantage of its long phosphorescence lifetime for the detection of SO_2 derivatives. **Ir-EA** is a specific and highly sensitive probe with low cytotoxicity and could be utilized for the imaging of exogenous and endogenous bisulfite derivatives in mitochondria of living cells by TPPIM and TPPLIM, which is better than most of iridium probes for bisulfite derivatives.

3　Conclusions

In this work, a new iridium(Ⅲ) probe **Ir-EA** with long phosphorescence lifetime has been designed and employed as a highly sensitive two-photon phosphorescent probe for real-time detection of bisulfite derivatives in vitro and *in vivo*. The probe **Ir-EA** displayed a rapid response to sulfur dioxide derivatives with significant phosphorescence enhancement, good selectivity, low detection limit (65 nmol·L^{-1}), and low cytotoxicity. For the first time, **Ir-EA** was successfully applied for detection of exogenous and endogenous bisulfite in living cells using TPPLIM. We anticipate that our study could provide a basis to develop a highly sensitive and selective probe for real-time detection of biological bisulfite derivatives in living cells, and we believe that this work would provide new methods and strategies to designing bioimaging reagents and bio-probes.

Supporting information is available at http://www.wjhxxb.cn

References:

[1] Chen T M, Kuschner W G, Gokhale J, et al. *Am. J. Med. Sci.*, **2007**,**333**:249-256

[2] Rich D Q, Schwartz J, Mittleman M A, et al. *Am. J. Epidemiol.*, **2005**,**161**:1123-1132

[3] Singh A, Agrawal M. *J. Environ. Biol.*, **2007**,**29**:15-24

[4] Sang N, Yun Y, Li H, et al. *Toxicol. Sci.*, **2010**,**114**:226-236

[5] Lee W J, Teschke K, Kauppinen T, et al. *Environ. Health Perspect.*, **2002**,**110**:991-995

[6] Shapiro R. *Mutat. Res.*: *Rev. Genet. Toxicol.*, **1977**,**39**:149-175

[7] Ji A J, Savon S R, Jacobsen D W. *Clin. Chem.*, **1995**,**41**:897-903

[8] Mitsuhashi H, Ikeuchi H, Yamashita S, et al. *Shock*, **2004**,**21**:99-102

[9] Tsuzuki T, Obaru K, Setoyama C, et al. *J. Mol. Biol.*, **1987**,**198**:21-31

[10]Mitsuhashi H, Yamashita S, Ikeuchi H, et al. *Shock*, **2005**,**24**:529-534

[11]Liang Y, Liu D, Ochs T, et al. *Lab. Invest.*, **2011**,**91**:12-23

[12]Wang X B, Jin H F, Tang C S, et al. *Eur. J. Pharmacol.*, **2011**,**670**:1-6

[13]Wang X B, Jin H F, Tang C S, et al. *Clin. Exp. Pharmacol. Physiol.*, **2010**,**37**:745-752

[14]Li X, Bazer F W, Gao H, et al. *Amino Acids*, **2009**,**37**:65-78

[15]Kajiyama H, Nojima Y, Mitsuhashi H, et al. *J. Am. Soc. Nephrol.*, **2000**,**11**:923-927

[16]Wang K N, Cao Q, Liu L Y, et al. *Chem. Sci.*, **2019**,**10**:10053-10064

[17]Theisen S, Hansch R, Kothe L, et al. *Biosens. Bioelectron.*, **2010**,**26**:175-181

[18]Zeng L, Gupta P, Chen Y, et al. *Chem. Soc. Rev.*, **2017**,**46**:5771-5804

[19]Sun M, Dai W, Liu D Q. *J. Mass Spectrom.*, **2008**,**43**:383-393

[20]Daunoravicius Z, Padarauskas A. *Electrophoresis*, **2002**,**23**:2439-2444

[21]Liang X, Zhong T, Quan B, et al. *Sens. Actuators B*, **2008**,**134**:25-30

[22]Yin J, Hu Y, Yoon J. *Chem. Soc. Rev.*, **2015**,**44**:4619-4644

[23]Vendrell M, Zhai D, Er J C, et al. *Chem. Rev.*, **2012**,**112**:4391-4420

[24]ZHAO Zhen-Sheng(赵振盛), GUO Xu-Dong(郭旭东), LI Sha-Yu(李沙瑜), et al. *Acta Chim. Sinica*(化学学报), **2016**,**74**:593-596

[25]Yang Y, Zhao Q, Feng W, et al. *Chem. Rev.*, **2013**,**113**:192-270

[26]Tang Y, Kong X, Xu A, et al. *Angew. Chem. Int. Ed.*, **2016**,**55**:3356-3359

[27]Wang J W, Wong A M, Flores J, et al. *Cell*, **2003**,**112**:271-282

[28]Gissibl T, Thiele S, Herkommer A, et al. *Nat. Photonics*, **2016**,**10**:554-560

[29]Cao D, Liu Z, Verwilst P, et al. *Chem. Rev.*, **2019**,**119**:10403-10519

[30]Zhao Q, Huang C, Li F. *Chem. Soc. Rev.*, **2011**,**40**:2508-2524

[31]Ma D L, He H Z, Leung K H, et al. *Angew. Chem. Int. Ed.*, **2013**,**52**:7666-7682

[32]He L, Tan C P, Ye R R, et al. *Angew. Chem. Int. Ed.*, **2014**,**53**:12137-12141

[33]Li Y, Tan C P, Zhang W, et al. *Biomaterials*, **2015**,**39**:95-104

[34]Li J, Pu K. *Chem. Soc. Rev.*, **2019**,**48**:38-71

[35]Guo Z, Park S, Yoon J, et al. *Chem. Soc. Rev.*, **2014**,**43**:16-29

[36]Zhang K Y, Gao P, Sun G, et al. *J. Am. Chem. Soc.*, **2018**,**140**:7827-7834

[37]Hao L, Li Z W, Zhang D Y, et al. *Chem. Sci.*, **2019**,**10**:1285-1293

[38]Zhao Q, Cao T, Li F, et al. *Organometallics*, **2007**,**26**:2077-2081

[39]Li G, Chen Y, Wang J, et al. *Chem. Sci.*, **2013**,**4**:4426-4433

[40]Li G, Chen Y, Wang J, et al. *Biomaterials*, **2015**,**63**:128-136

[41]Wang K N, Zhu Y, Xing M, et al. *Sens. Actuators B*, **2019**,**295**:215-222

[42]Liu J B, Yang C, Ko C N, et al. *Sens. Actuators B*, **2017**,**243**:971-976

[43]Li X, Zeng R, Xie C, et al. *Dyes Pigm.*, **2019**,**165**:128-136

[44]Gao H, Qi H, Peng Y, et al. *Analyst*, **2018**,**143**:3670-3676

[45]Liu Z, Guo S, Piao J, et al. *RSC Adv.*, **2014**,**4**:54554-54557

[46]Zhang Y, Guan L, Yu H, et al. *Anal. Chem.*, **2016**,**88**:4426-4431

[47]Zhang W, Liu T, Huo F, et al. *Anal. Chem.*, **2017**,**89**:8079-8083

[48]Li C, Yu M, Sun Y, et al. *J. Am. Chem. Soc.*, **2011**,**133**:11231-11239

[49]Liu Z, Zhou X, Miao Y, et al. *Angew. Chem. Int. Ed.*, **2017**,**56**:5812-5816

[50]Sheldrick G M. *SHELX*-97, *Program for the Solution and the Refinement of Crystal Structures*, University of Göttingen, Germany, **1997**.

[51]Zhang F, Liang X, Zhang W, et al. *Biosens. Bioelectron.*, **2017**,**87**:1005-1011

[52]He L, Qiao J, Duan L, et al. *Adv. Funct. Mater.*, **2009**,**19**:2950-2960

[53]Jiao X, Li Y, Niu J, et al. *Anal. Chem.*, **2018**,**90**:533-555

[54]Lin V S, Chen W, Xian M, et al. *Chem. Soc. Rev.*, **2015**,**44**:4596-4618

[55]Wu J, Pan J, Ye Z, et al. *Sens. Actuators B*, **2018**,**274**:274-284

[56]Hou J T, Ren W X, Li K, et al. *Chem. Soc. Rev.*, **2017**,**46**:2076-2090

[57]Cipollone R, Ascenzi P, Tomao P, et al. *J. Mol. Microbiol. Biotechnol.*, **2008**,**15**:199-211

[58]Ploegman J H, Drent G, Kalk K H, et al. *Nature*, **1978**,**273**:120-124

[59]Ramasamy S, Singh S, Taniere P, et al. *Am. J. Physiol.: Gastrointest. Liver Physiol.*, **2006**,**291**:288-296

[60]Malliopoulou V, Rakitzis E, Malliopoulou T. *Anticancer Res.*, **1989**,**9**:1133-1136

[61]Zhang K Y, Yu Q, Wei H, et al. *Chem. Rev.*, **2018**,**118**:1770-1839

[62]Nasevicius A, Ekker S C. *Nat. Genet.*, **2000**,**26**:216-220

[63]Zon L I, Peterson R T. *Nat. Rev. Drug Discovery*, **2005**,**4**:35-44

[64]Lieschke G J, Currie P D. *Nat. Rev. Genet.*, **2007**,**8**:353-367